http://www.scar.ac.cn
Sciences in Cold and Arid Regions
2012, 4(3): 0211–0221
DOI: 10.3724/SP.J.1226.2012.00211

Spatial-temporal variations of vegetation cover in Yellow River Basin of China during 1998–2008

Qin Nie [1,2], JianHua Xu [1*], Zhuo Li [1], YuLian Hong [1]

1. The Research Center for East-West Cooperation in China, The Key Lab of GIScience of the Education Ministry PRC, East China Normal University, Shanghai 200241, China
2. School of Environment and Planning, Liaocheng University, Liaocheng, Shandong 252059, China

*Correspondence to: Prof. JianHua Xu, The Research Center for East-West Cooperation in China, East China Normal University, Shanghai 200241, China. Tel: +86-21-62232146; Email: jhxu@geo.ecnu.edu.cn

Received: December 23, 2011 Accepted: March 15, 2012

ABSTRACT

Using an integrated method combining wavelet analysis and non-parameter Mann-Kendall test, this paper analyzed spatial-temporal variations of vegetation cover in the Yellow River Basin based on SPOT-VEG images from 1998 to 2008. The results indicate: (1) Vegetation cover presented marked seasonal variation during the study period, with minima around winter and maxima in summer. The detail component *D*5 (with semi-period of 240 days) has presented a major contribution to the intra-annual variability. Forest vegetation presents a marked decreasing trend, while alpine shrubs, meadow, typical steppe, desert steppe, and forest (meadow) steppe vegetation all show a marked increasing trend. (2) Mean vegetation amount increased from the upper to lower reaches of the basin. It is low in the Ordos Plateau and Loess Plateau, and high in the southern Loess Plateau and the lower reaches. Amplitude of the annual phenological cycle presents an opposite pattern in spatial distribution with that of the mean vegetation amount. (3) Vegetation cover presented a dominant positive inter-annual change trend, which implies that the eco-environment in the region has steadily improved. Only a few areas show a negative trend, which are located in the upper reaches and the southern Loess Plateau.
Keywords: vegetation coverage dynamic; NDVI time series; Yellow River Basin; wavelet analysis; Mann-Kendall test

1. Introduction

Vegetation plays a vital role in the carbon-water-energy cycle of terrestrial ecosystems (Xiao and Moody, 2005), and has been an indicator for global change research (Sun *et al*., 1998; Cao *et al*., 2011). Quantifying the magnitude of vegetation cover change therefore is crucial to understanding ecosystem dynamics, especially in regions that are sensitive to global change. The Yellow River Basin (YRB), as one of the seven longest river basins in China, spans across arid, semi-arid, and semi-humid climate zones, which results in rich vegetation types, but with a very fragile ecosystem in part of the basin. Specially, drought and flooding disasters frequently occur in this basin, which is in response to global change. It is, therefore, important to gain a deep and thorough understanding of the vegetation dynamics in order to monitor environmental dynamics and establish proper environmental conservation strategies for sustainable development in the region. Our primary interest lies in the spatial-temporal variations of vegetation in YRB.

In the last 20 years, numerous studies have evaluated the vegetation dynamics in YRB, but the majority is of the single-time scale analysis. Vegetation cover is usually characterized by patterns like seasonal variations, long-term trends and localized abrupt changes resulting from disturbance events. Therefore, a multiple time-scale analysis on vegetation dynamics is essential and meaningful.

To date, because of the analysis ability of large areas with a high temporal frequency, satellite remote sensing

has long been considered as an ideal technology for the study of vegetation dynamics. An example is SPOT production, which can provide the required time-series of satellite images to extract key phenological parameters and monitor vegetation dynamic trends. Among the surface parameters extracted from remote sensing data, the Normalized Difference Vegetation Index (NDVI), a spectral index linearly related to the fraction of the photosynthetically active radiation (400–700 nm) intercepted by the canopy, is fundamental to remote sensing of vegetation phenology and to extract numerical observations related to vegetation dynamics (Tucker and Sellers, 1986; Hall-Beyer, 2003; Pettorelli *et al*., 2005; Srur *et al*., 2012). It has become a de facto standard approach for research in environmental science, ecology and agriculture (Asrar *et al*., 1984; Garty *et al*., 2001; Li *et al*., 2005; Zhang *et al*., 2006; Giannico, 2007; Diodato and Bellocchi, 2008; Jarlan *et al*., 2008).

Numerous case studies in different countries and regions have also been conducted to evaluate vegetation dynamics. As a result, several methodologies have been developed to monitor vegetation dynamics from multi-temporal data, including statistical methods such as principal component analysis (Hirosawa *et al*., 1996; Hall-Beyer, 2003) and curve fitting (Jonsson and Eklundh, 2004), as well as spectral-frequency techniques such as Fourier analysis (Azzali and Menenti, 2000; Stockli and Vidale, 2004), harmonic analysis (Jakubauskas *et al*., 2001) and wavelet transform (Yang *et al*., 2012). However, it has proven difficult to achieve a thorough understanding of the vegetation dynamic mechanism. Specifically, there is still a lack of effective means available to reveal the characteristic underlying vegetation dynamics and quantify the magnitude of vegetation dynamics at different time scales.

In this paper, using SPOT-VEG image-based NDVI data (from April of 1998 to July of 2008), the spatial-temporal variations of vegetation coverage were investigated from multiple time scales by means of an integrated method combining wavelet analysis and non-parameter Mann-Kendall test. Usually, wavelet analysis is used as a multi-resolution analysis method, *i.e*., it can decompose the time series of NDVI into different temporal components, such as intra- and inter-annual variations, and allow for characterizing these vegetation dynamics at several temporal scales (Yang *et al*., 2012). Furthermore, on the one hand, the intra-annual variation associated with seasonal changes can be processed to define several key features in relation with vegetation dynamics (Martínez and Gilabert, 2009), like mean and minimum NDVI values, amplitude of the phonological cycle, and date of maximum NDVI. On the other hand, inter-annual components can be used to calculate the parameter of mean NDVI value and to identify vegetation change trend by trend analysis (Martínez and Gilabert, 2009). All these key parameters are required for a better understanding of vegetation dynamics (IGBP 1997; Turner *et al*., 2007). This study attempts to answer the following questions: (1) What is the characteristics of NDVI variation at different time scales? *i.e*., the characteristics of intra- and inter-annual vegetation dynamics. (2) How is the spatial distribution with respect to key vegetation parameters, such as mean and minimum NDVI, and the amplitude of the annual phenological cycle? (3) When do maximum NDVI values appear during the study period? (4) How is the trend of inter-annual vegetation variation?

2. Materials and data

2.1. Study area

Originating in the Bayan Har Mountains in Qinghai Province of western China, the Yellow River is the second-longest river in China and the sixth-longest in the world, with an estimated length of 5,464 km. It flows through nine provinces of China and empties into the Bohai Sea. The Yellow River Basin ranges between 96°–119°E and 32°–42°N with an area of 794,712 km^2, an east-west extent of 1,900 km, and a north-south extent of 1,100 km (Yang *et al*., 2002). This basin has a continental climate, with semi-humid climate in the south-east, semi-arid climate in the middle, and arid climate in the north-west. The average annual precipitation in the basin is between 200 and 600 mm, and drought is the basic characteristic. As a result, the eco-environment in the basin is complex and sensitive to typical continental climate. Together with the complex geomorphic type and inconsistent topography, the vegetation type is diverse (Figure 1). From east to west, the vegetation consists of warm temperature zone forest, temperate zone forest (meadow) steppe, temperature zone typical steppe, temperate zone desert steppe, temperate zone shrub and semi-shrub desert, alpine shrubs and meadow, and alpine steppe.

2.2. Data description

NDVI data from 1998 to 2008 in the Yellow River Basin were obtained from the Image Processing and Filing Center of VITO Institute, Belgium, which has been improved by applying atmospheric correction, cloud removal, and bi-directional reflectance distribution function (BRDF) correction (Morawitz, 2006). Each 10-day NDVI data was synthesized using a revised Maximum Value Composites (MVC) method (*i.e*., Max($NDVI_1$, $NDVI_2$, …, $NDVI_i$)), meaning that for each location, the pixel with the highest NDVI value during ten consecutive days was selected for the synthetic image. The 10-day periods of synthetic SPOT-VGE scenes were defined as from date 1 to date 10, date 11 to date 20, and date 21 to the end of each month. The spatial resolution

was 1km×1km, nearly as a constant across the whole 2,250-km swath, which meant that there was almost no distortion at the image edge (Maisongrande *et al*., 2004).

In this research, a time series of 372 SPOT-VEG scenes was obtained, covering the period from April of 1998 to July of 2008. SPOT-VEG images record the digital number (DN) between 0 and 255. For the convenience of display, the grey value of every pixel is linearly stretched by NDVI=DN×0.004−0.1, which converts the data range to [0, 1].

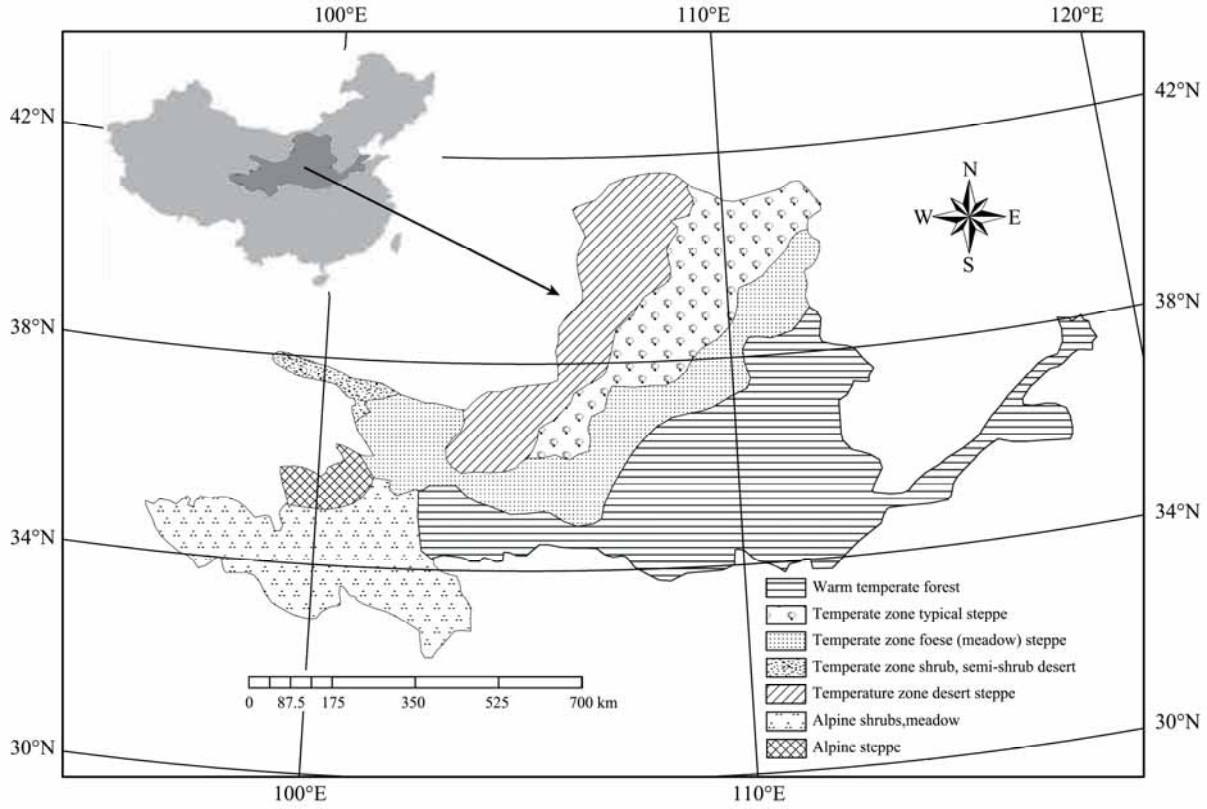

Figure 1 Types of vegetation cover in the Yellow River Basin

3. Methodology

Three steps were taken to research the spatial-temporal variations of vegetation cover in the Yellow River Basin. Firstly, a wavelet transform was applied to NDVI time series to decompose the original series into the inter-annual and intra-annual series. Secondly, different key features, such as mean NDVI value, minimum NDVI value, amplitude of the phonological cycle, and date of maximum NDVI, which are related to vegetation phenology, were extracted and analyzed. Lastly, based on the inter-annual components, the non-parametric Mann-Kendall test was used to describe vegetation dynamic trend, and slope Q, considered as the magnitude of the land-cover change, was calculated and analyzed.

3.1. Wavelet transform

Our previous studies have validated that wavelet analysis is a useful tool for analyzing climatic, hydrological and economic variables (Xu *et al*., 2004; 2010; 2011a, b). In this study, NDVI time series will be decomposed and reconstructed by using wavelet transform.

Let the signal $f(t)$ be a real-valued function in the time dimension. Its continuous wavelet transform (CWT) with respect to the wavelet basis function, $\psi_{a,b}(t)$, can be defined as:

$$\psi(a,b) = \int_{-\infty}^{\infty} \overline{\psi}_{a,b}(t) f(t) dt = \frac{1}{\sqrt{a}} \int_{-\infty}^{\infty} \overline{\psi}_{a,b}\left(\frac{t-b}{a}\right) f(t) dt \quad (1)$$

where $\psi_{a,b}$ is the mother wavelet complex conjugate. For each scale, the result of the wavelet transform is a set of coefficients associated with different locations (Lindsay *et al*., 1996), a and b is parameter of time scale and time central, respectively.

By wavelet decomposition on the basis of the discrete wavelet transform (DWT), the nonlinear pattern of a time series $x(t)$ can be analyzed at multiple scales. DWT is defined by taking discrete values of a and b. The full DWT for signal $x(t)$ can be represented as (Mallat, 1989):

$$x(t)=\sum_{k}\mu_{j_0,k}\phi_{j_0,k}(t)+\sum_{j=1}^{j_0}\sum_{k}\omega_{j,k}\psi_{j,k}(t) \quad (2)$$

where $\phi_{j_0,k}$ and $\psi_{j,k}(t)$ are the flexing and parallel shift of the basic scaling function, $\phi(t)$, and the mother wavelet function, $\psi(t)$, and $\mu_{j_0,k}$ ($j<j_0$) and $\omega_{j,k}$ are the scaling coefficients and the wavelet coefficients, respectively.

3.2. Mann-Kendall test

The Mann-Kendall test is usually used to examine the significance of temporal trends from time series data. It has been widely used to assess the significance of trend in hydrological and climate time series, such as runoff, temperature, and precipitation (Xu and Zhang, 2006; Xu *et al*., 2009). Cao *et al.* (2012) substantiated the validity of the Mann-Kendall test for examining vegetation cover trend.

The statistic of the Mann-Kendall statistical test, Z, is expressed as:

$$Z=\begin{cases}\dfrac{S-1}{\sqrt{\mathrm{var}(S)}}, S>0\\ 0, S=0\\ \dfrac{S+1}{\sqrt{\mathrm{var}(S)}}, S<0\end{cases} \quad (3)$$

$$S=\sum_{i=1}^{n-1}\sum_{k=i+1}^{n}\mathrm{sgn}(x_k-x_i) \quad (4)$$

where

$$\mathrm{sgn}(\theta)=\begin{cases}1, & \theta>0\\ 0, & \theta=0\\ -1, & \theta<0\end{cases} \quad (5)$$

$$\mathrm{var}(S)=n(n-1)(2n+5)/18 \quad (6)$$

where x_k and x_i are the sequential data values, and n is data length.

The index for measurement of trend, *i.e*., the inclination is expressed as follows:

$$Q=\mathrm{Median}\left(\frac{x_i-x_j}{i-j}\right) \quad (7)$$

where $1<j<i<n$, and a positive Q denotes a rising trend, while a negative Q means a decreasing trend.

The Mann-Kendall test can be used in the following manner: for the null hypothesis of H_0, $\beta=0$, if $|Z|>Z_{(1-\alpha)/2}$, then the null hypothesis is refused, where, $Z_{(1-\alpha)/2}$ is the standard normal variance, and a is the significance level for the test.

In this study, the Mann-Kendall test will be applied to the inter-annual components derived from the wavelet decomposition, and be used to examine the significance of the total NDVI time series during the study period.

4. Experimental procedure

In this study, the Sym8 orthogonal discrete wavelet has been chosen as mother wavelet due to: (1) existence of a scaling function for numerical implementation of the wavelet transform; (2) its regularity condition that assures the smoothness of the reconstructed signal; (3) ease of implementation and (4) low cost computation.

The time series of NDVI is usually non-stationary, *i.e*., they present different frequency components, such as seasonal variations, long-term and short-term fluctuations. In order to select the most appropriate scales for the study of the different components, the scale and frequency need to be connected (Martínez and Gilabert, 2009). A convenient way is to characterize the dominant frequency of the wavelet by defining a purely periodic signal of period (Meyers *et al*., 1993; Abry, 1997):

$$P=\frac{\alpha\Delta t}{Vc} \quad (8)$$

where α is the scale, Δt is the sampling period, and Vc is the center frequency of the wavelet in Hz. In this study, the sampling period is ten days, and the center frequency of Sym8 wavelet is 0.66667. Table 1 shows the period and semi-period corresponding to the different scales for the Sym8 wavelet. Period P refers to the global temporal scale used in the wavelet computation. The time scale has been selected according to the semi-period since it accounts for differences between months and years, respectively (Martínez and Gilabert, 2009).

Table 1 Period (P) and semi-period ($P/2$) corresponding to the wavelet decomposition levels

Level (j)	Scale (α)	P (days)	P/2 (days)
1	2	30	15
2	4	60	30
3	8	120	60
4	16	240	120
5	32	480	240
6	64	960	480

Since $P/2$=480 days for $\alpha=2^6$, the approximation component for level 6, $A6$, provides information about the inter-annual variability over the considered period. Meanwhile, detail components at levels j=2, 3, …, 6, are attributable to changes at scales: $D2$(16–30 days), $D3$(31–60 days), $D4$(61–120 days), $D5$(121–240 days), and $D6$(241–480 days). The first-level has been discarded because it accounts for high frequency variations (< 1 month), which are mostly due to temporal noise. Therefore, the detail components, $D2$, $D3$, ..., $D6$, with semi-periods ranging from 30 to 480 days, have been selected to analyze the intra-annual vegetation dynamics.

In summary, the components employed in this study are: (1) the variability component, $V=D2+D3+\ldots+D6$, which refers to the sum of the detail components up to level six and can be regarded as the total intra-annual variability; (2) detail component $D5$, which is related to semi-annual variations because its semi-period is 240 days; and (3) the $A6$ component, which describes inter-annual changes. These scales were interrelated with each other. Usually, the fine scale corresponds to rapidly changing details (high frequency), whereas coarse scale corresponds to slowly changing coarse features (low frequency). NDVI series is studied at a coarse resolution (such as inter-annual scale) to obtain an overall view of vegetation dynamics and at incrementally finer resolutions (such as intra-annual scale) to see increasingly finer details.

The experimental procedure to study the vegetation dynamics in YRB is divided into three steps. Firstly, wavelet transform is applied to the NDVI time series to decompose the original series into the inter-annual $A6$ and intra-annual V and $D5$ series.

The second step consists of extracting different key features (Table 2) from the above series (*i.e*. inter- and intra-annual series), including mean NDVI value, minimum NDVI value, amplitude of the phonological cycle, and dates of maximum NDVI, which are related to vegetation phenology. All these parameters are potentially useful in studying vegetation dynamics. Mean NDVI value is an indicator of the mean vegetation amount during the analyzed time range, whereas minimum NDVI value ($NDVI_{\min}$) quantifies the minimum level of the NDVI. $\Delta NDVI$ is the amplitude of the annual phenological cycle, without including noise due to the presence of outliers in the original signal. Data of the maximum NDVI, $T_{\max}$, is related with the phenological cycle of each vegetation cover type, and considered as an important feature to characterize vegetation dynamics.

The third step consists of identification of vegetation cover change trend. The trend analysis is performed on the inter-annual component $A6$, which is not affected by seasonal variability. In the present case, the non-parameter Mann-Kendall test has been used to detect and quantify the trends. In addition, slope Q of the trends, which are considered to be a good approximation to evaluate the net change throughout the studied time range, have been obtained based on Sen's method (Sen, 1968).

The procedure has been applied on the per-pixel basis in the region. NDVI time series are obtained based on ENVI software and IDL language. Wavelet analysis and the Mann-Kendall test are executed based on Matlab software.

Table 2 Key features computed from wavelet transform to study vegetation dynamics

Parameter	Description	Meaning
$\overline{NDVI}$	Mean of the inter-annual component: $\overline{NDVI} = \overline{A6}$	Mean NDVI level of vegetation during the period
$NDVI_{\min}$	Percentile 10% of the sum of mean inter-annual and intra-annual variability: $NDVI_{\min} \equiv P_{10}(\overline{A6} + V)$	Minimum NDVI level reached during the period
$\Delta NDVI$	Range of percentiles 10% and 90% for the intra-annual variability: $\Delta NDVI \equiv R_{10,90}(V)$	Amplitude of the annual phenological cycle
$T_{\max}$	Timing of the maximum NDVI corresponding to the $D5$ component.	Date of maximum NDVI
Q	Slope of the inter-annual component ($A6$) obtained from the Sen's method	Trend in the data series: magnitude of the land-cover change

5. Results and discussion

5.1. Vegetation cover dynamic

Six case pixels belonging to different vegetation types were chosen to study the intra- and inter-annual NDVI dynamic.

5.1.1 The intra-annual vegetation cover dynamic

The intra-annual V for the six case pixels are presented in Figure 2. The intra-annual series show a seasonal variation for each cover type. Specifically, temperate zone typical steppe vegetation (Figure 2c) and temperate zone shrub, semi-shrub desert vegetation (Figure 2d) presented the most marked seasonality, with maximum value in summer and minima in winter. The other vegetation types (Figures 2a, 2b, 2e, 2f) also presented marked seasonal variation, with minima around winter and maxima in summer. The amplitude of intra-annual variation was lower for warm temperate zone forest (Figure 2b), whereas higher for alpine shrubs, meadow

(Figure 2a).

Preliminary analysis has also been done to quantify how much each scale contributes to the overall variability in the original NDVI time series by the wavelet variance. Normalized wavelet variance versus the scale level for the six selected pixels (Figure 3) indicates that total wavelet variance of the signal was dominated by the fraction of the signal attributable to scale levels between 4 and 5. More than 35% of the total variance was accounted for by scale level 5, reaching values up to 60% for temperate zone shrub, and semi-shrub desert vegetation.

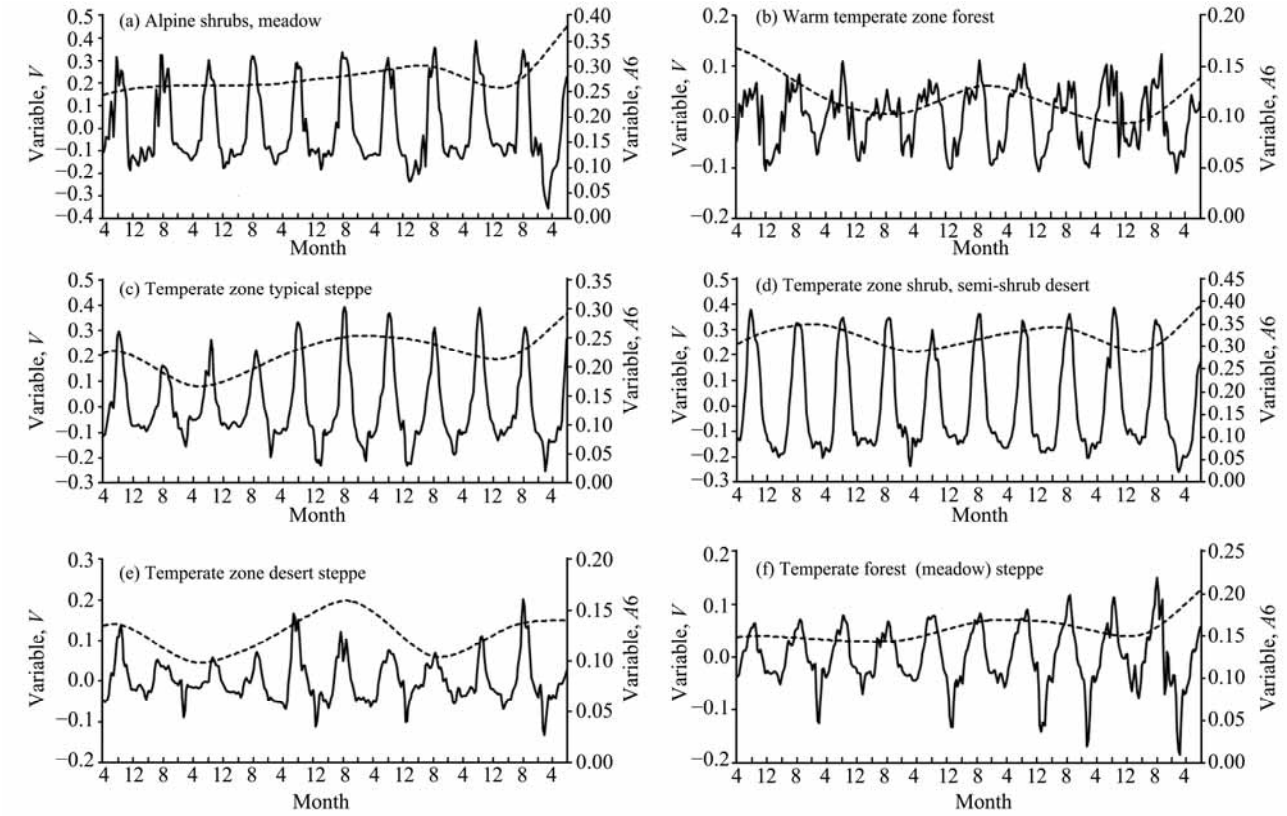

Figure 2 Intra-annual variability component (V, solid line) and inter-annual component for level 6 ($A6$, dashed line) variations for six case pixels

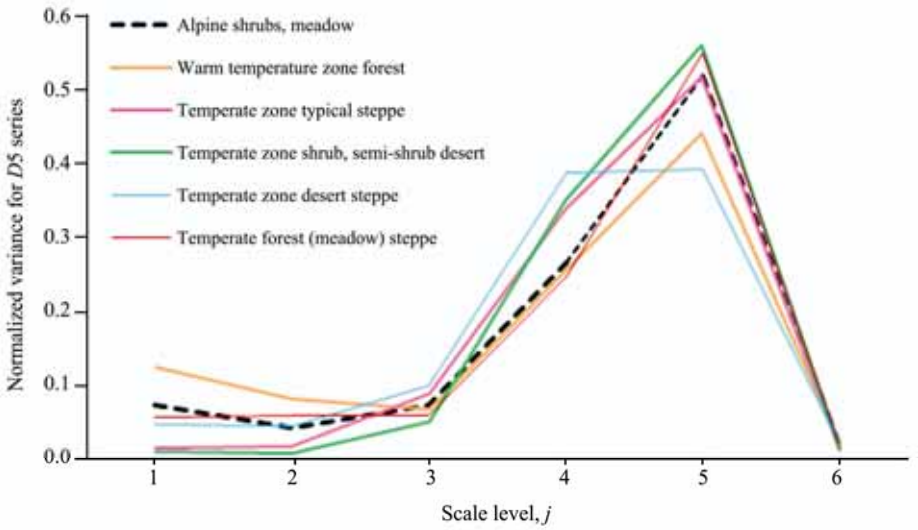

Figure 3 Normalized wavelet variance versus the scale level for the six case pixels

From the aforementioned analysis, detail component *D*5 presented a major contribution to the intra-annual variability. Figure 4 shows series *D*5 for the six pixels. They all presented a similar pattern of intra-annual variability, with an absolute NDVI maximum in summer for every vegetation type.

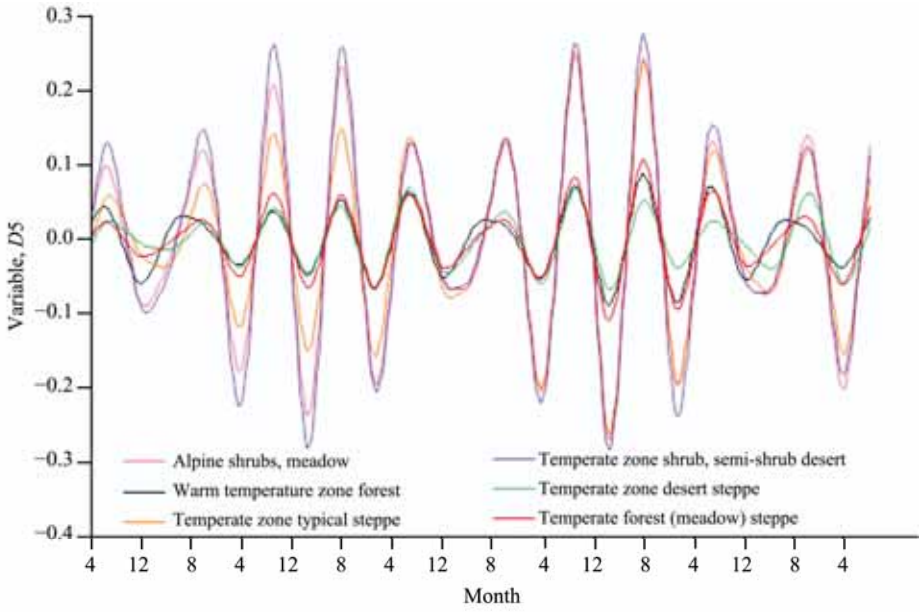

Figure 4 Series *D*5 for the six case pixels

5.1.2 The inter-annual vegetation cover dynamic

The shapes of *A*6 curves (Figure 2) for the six case pixels were related to inter-annual changes. The curves for alpine shrubs, meadow vegetation (Figure 2a) and temperate zone forest (meadow) steppe vegetation (Figure 2f) were flatter, showing weak relative change. The other four vegetation types presented high inter-annual variability. In addition, a general increase of the vegetation amount has been observed, except warm temperate zone forest vegetation (Figure 2b) showing a decrease. A Mann-Kendall test has been applied to the inter-annual series and slope *Q* has been derived from Sen's slope method. The results (Table 3), which are significant for five of the selected six pixels, indicate positive and negative trends. Forest vegetation (II) presented a marked decreasing trend, whereas a remarkable increasing trend were presented in alpine shrubs, meadow (I), typical steppe (III), desert steppe (V), and forest (meadow) steppe vegetation (VI). However, the *Z* value (the statistic of Mann-Kendall statistical test) for shrub, and semi-shrub desert vegetation (IV) was not significant. These trends were in accord with that presented by the curves of inter-annual series.

Comparing these intra-annual curves of *V* with the corresponding inter-annual curves of *A*6, the intra-annual variations were found to keep the trend of the inter-annual variations, but the nonlinear characteristics of NDVI variations were more identifiable. Therefore, the characteristic of vegetation dynamics was dependent on temporal scales.

Table 3 Trend analysis from the non-parameter Mann-Kendall test for the selected pixels

Vegetation type	I	II	III	IV	V	VI
Z	19.06	−10.83991591	10.47270161	−1.454252106	5.67054	11.37405
P	1	1	1	0	1	1
Q ($\times 10^5$)	15.2120038	−9.56962592	15.56920375	−1.585896479	4.696275	6.188991

I: Alpine shrubs, meadow; II: Forest; III: Typical steppe; IV: Shrub, semi-shrub desert; V: Desert steppe; VI: Forest (meadow) steppe. *P*=1 means significant at 99% level; *P*=0 means insignificant.

5.1.3 Key features of vegetation dynamics

Applying the wavelet transform to each pixel, a series of images can be calculated to study NDVI dynamics in YRB. Figures 5–8 show the features of mean NDVI value, minimum NDVI value, amplitude of the phonological cycle, and dates of the maximum NDVI.

Figure 5 shows much contrasted information about the mean vegetation amount during the analyzed time range. Roughly speaking, mean vegetation amount during 1998–2008 increased from the upper to lower reaches of the basin. Minimum values occurred in the Ordos

Plateau and north Loess Plateau, and maximum values in the southern Loess Plateau and the lower reaches of YRB. In addition, the mean amount in the eastern Tibetan Plateau was high.

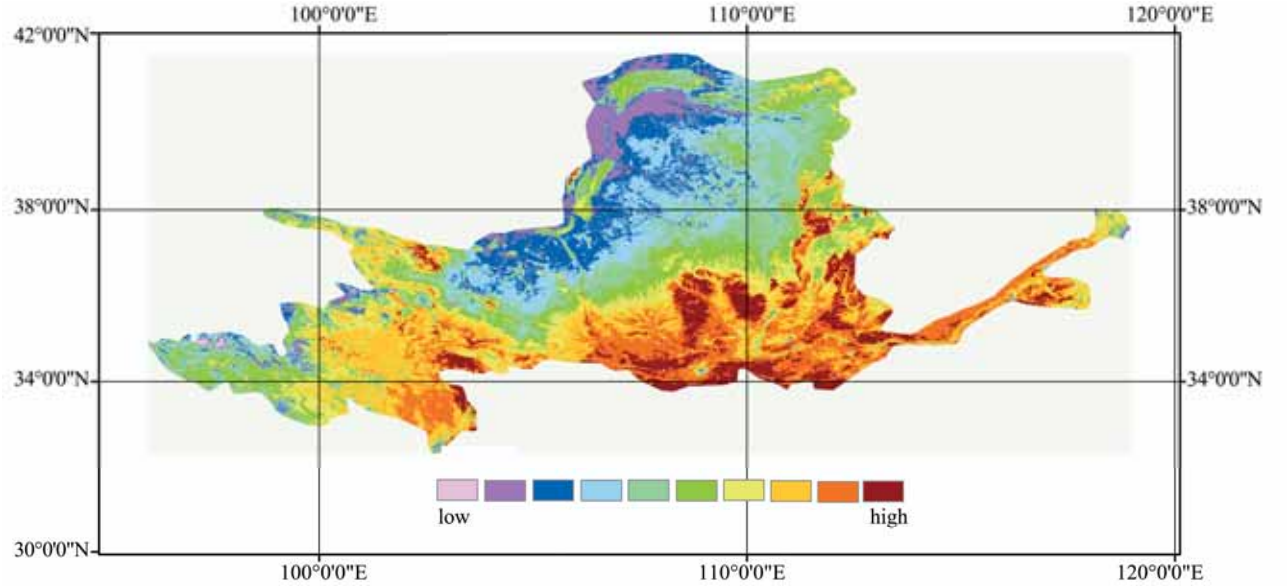

Figure 5 The mean of NDVI

Figure 6 shows the minimum level of NDVI for each pixel during the study period. The minimum levels of NDVI were low in the eastern Tibetan Plateau, the southern Loess Plateau and the lower reaches, and the minimum level in the Ordos Plateau and the north Loess Plateau were high.

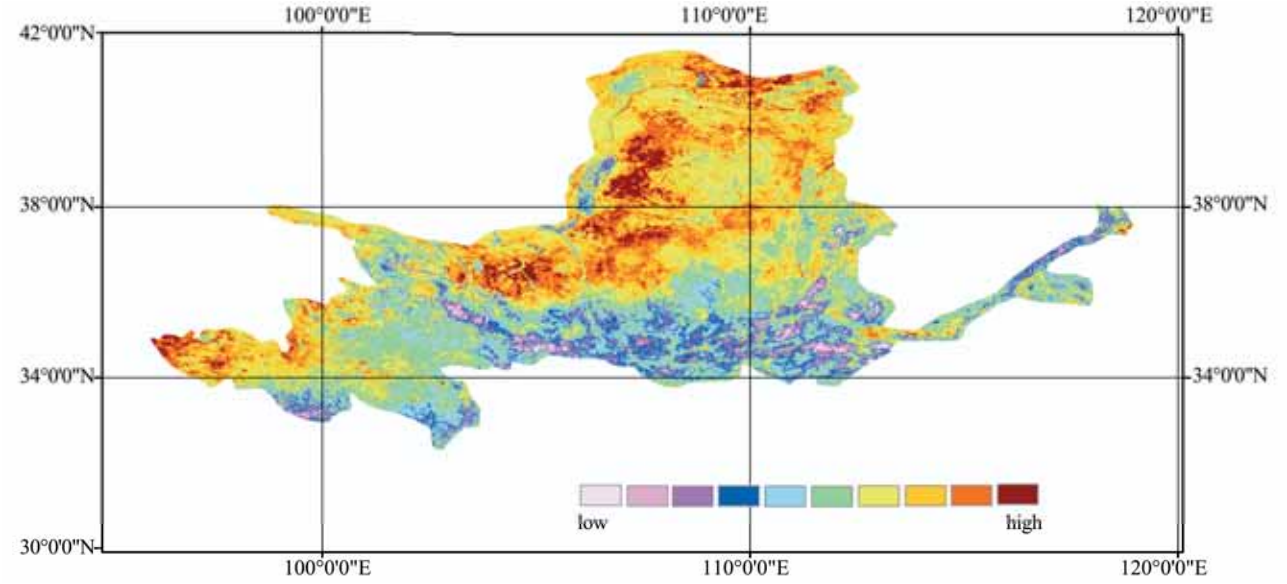

Figure 6 The minimum of NDVI

Figure 7 provides the amplitude of the annual phenological cycle. It presented an opposite pattern to that of the mean vegetation amount. We can see that the amplitude was high in arid and semi-arid regions, especially in the Ordos Plateau and the Loess Plateau. In contrast, the amplitude was low in the southern Loess Plateau and the semi-humid regions.

Figure 8 shows the distribution pattern of the maximum NDVI during the 11 years. Most pixels presented the maximum values between June and August. That is to say, most vegetation is summer-peaking vegetation. Beyond that, spring-peaking and autumn-peaking vegetation were scattered in the upper and lower reach of the basin.

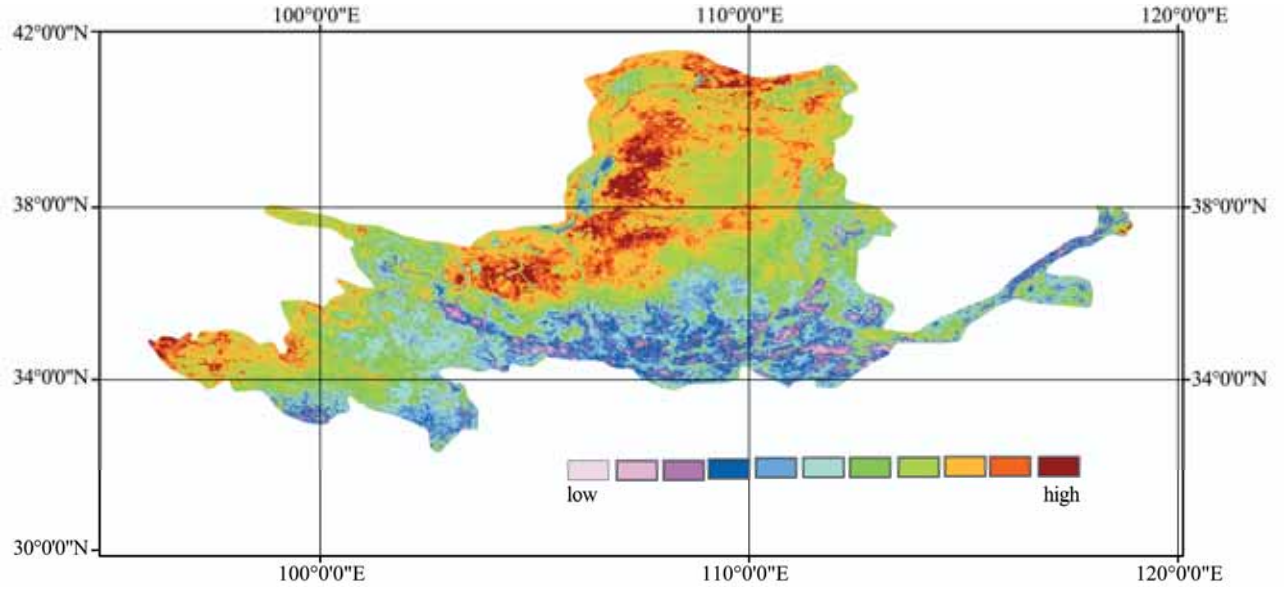

Figure 7 The amplitude of the annual phenological cycle, Δ*NDVI*

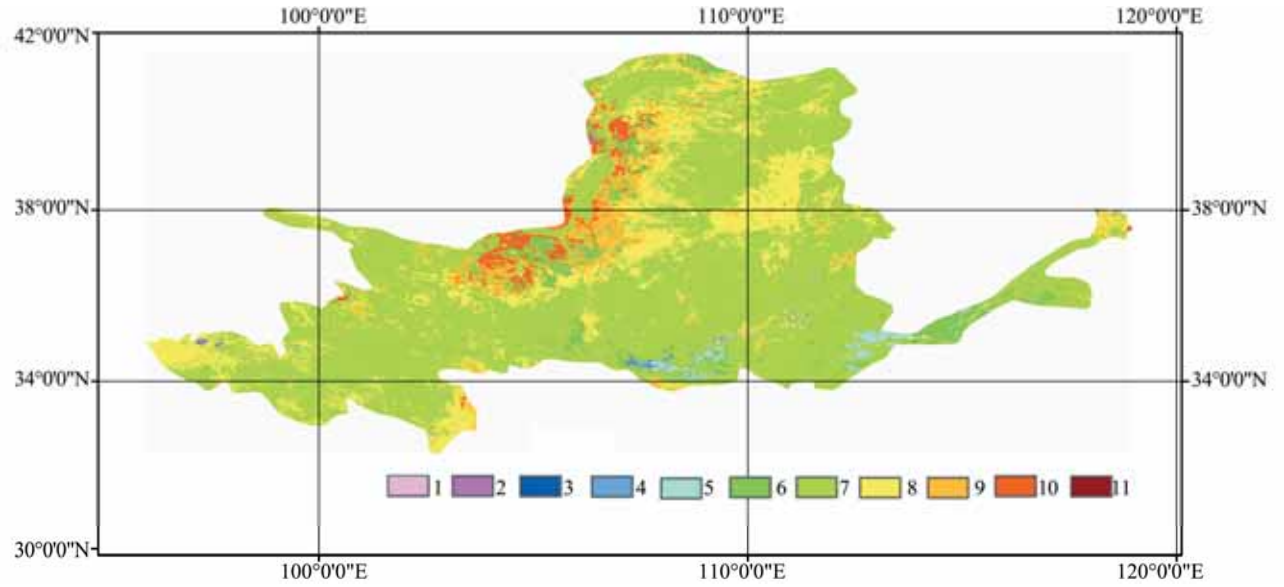

Figure 8 The timing of the maximum NDVI, T_{max}

5.2. Inter-annual trend of vegetation cover

Figure 9 shows slope Q derived from Sen's slope method for each pixel. The results are significant for most pixels, and the positive trends were dominant, accounting for 62.2% for the total pixels, with only a few areas with negative trends, accounting for only 20.4%. In other words, the vegetation cover presented a dominant positive change trend, which implies that the eco-environment in the region has steadily improved. The areas showing a negative trend located in the upper reaches and the southern Loess Plateau.

6. Conclusions

Summarizing the above results and discussion, we elicited the basic conclusions as follows:

(1) The wavelet transform has the potential to capture and describe both intra- and inter-annual changes in NDVI data. The variability series (V), *i.e.*, the sum of the detail components from levels 2 to 6, can be used to represent the total intra-annual variability, and the $A6$ series (with semi-period of 480 days) is related to inter-annual changes. Some key features, such as mean and minimum NDVI values, amplitude of the phonological cycle, date of maximum NDVI, and magnitude of the land-cover change, can be calculated to quantitatively characterize the vegetation phenology and the inter-annual change trends. These provide a new insight into the study of vegetation dynamics from NDVI data.

(2) The characteristics of vegetation dynamics are de-

pendent on temporal scales. The intra-annual series for the six case pixels all present marked seasonal variation, with minima around winter and maxima in summer, especially the pixels in temperate zone typical steppe vegetation and temperate zone shrub, semi-shrub desert vegetation, presenting the most marked seasonality. The amplitude of intra-annual variation is lower for warm temperate zone forest, whereas higher for alpine shrubs, meadow. The detail component *D*5 presents a major contribution to the intra-annual variability. The inter-annual curves for the case pixels in alpine shrubs, meadow type and temperate zone forest (meadow) steppe type show weak relative change, however the other four case series present high inter-annual variability. The case pixel in forest vegetation presents a marked decreasing trend, while the case pixel in shrub, semi-shrub desert vegetation presents an increasing trend, but the increase is not significant, and the other four case pixels all show a marked inter-annual increasing trend.

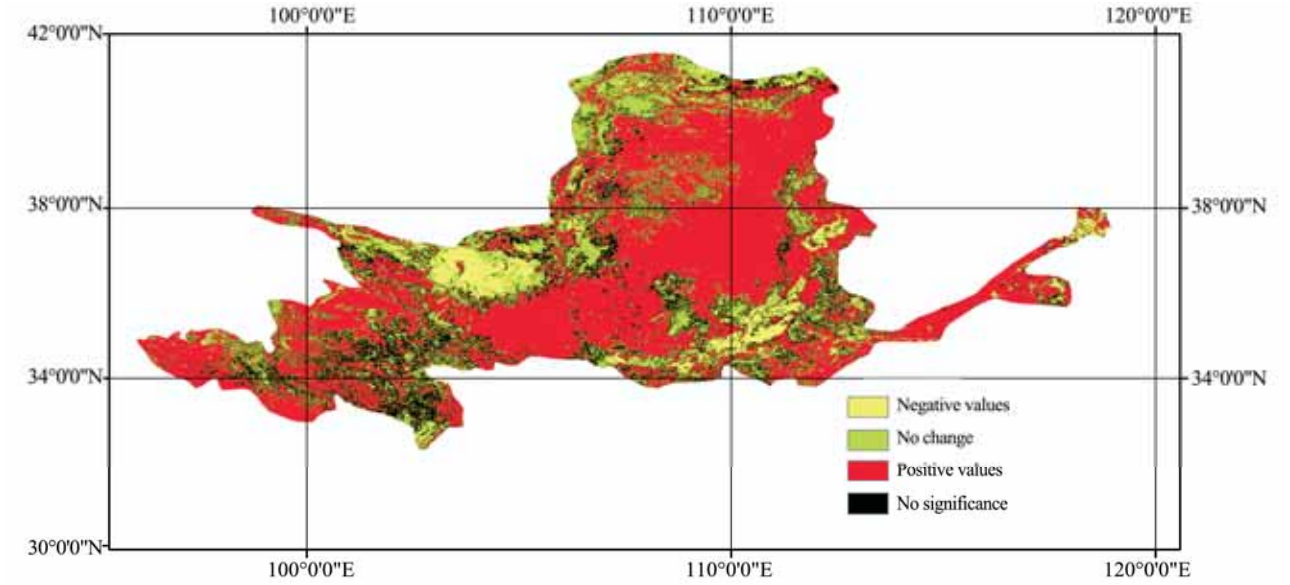

Figure 9 Slope of the inter-annual component, *Q*

(3) The mean vegetation amount during 1998–2008 increased from the upper to lower reaches of the basin. It is low in the Ordos Plateau and the Loess Plateau, and high in the southern Loess Plateau and the lower reaches of YRB. In addition, the mean values in the eastern Tibetan Plateau are high. Minimum NDVI levels for each pixel are low in the eastern Tibetan Plateau, southern Loess Plateau and the lower reaches, and the minimum levels in the Ordos Plateau and the north Loess Plateau are high. The amplitude of the annual phenological cycle is high in arid and semi-arid regions, highest especially in the Ordos Plateau and Loess Plateau. In contrast, the amplitude is low in the south of Loess Plateau and the semi-humid regions. Most pixels present maximum NDVI values in June or August, which means that most vegetation is summer-peaking vegetation. In addition, the spring-peaking and autumn-peaking vegetation are scattered in the upper and lower reaches of the basin.

(4) The eco-environment in the region has steadily improved. The vegetation cover presented a dominant positive change trend, with only a few areas showing a negative trend, which are located in the upper reaches of the basin and the southern Loess Plateau.

Acknowledgments:

The authors are very thankful to two reviewers for their helpful suggestions. This work was supported by National Natural Science Foundation of China (Grant Nos. 41130525, 41040015).

REFERENCES

Abry P, 1997. Ondelettes et turbulence. In: Diderot M (ed.). Multirésolutions algorithms de décomposition, invariance déchelle et signaux de pression. Paris, pp. 268.

Asrar G, Fuchs M, Kanemasu ET, Hatfield JL, 1984. Estimating absorbed photosynthetic radiation and leaf area index from spectral reflectance in wheat. Agronomy Journal, 76: 300–306.

Azzali S, Menenti M, 2000. Mapping vegetation-soil-climate complexes in southern Africa using temporal Fourier analysis of NOAA AVHRR NDVI data. International Journal of Remote Sensing, 21(5): 973–996. DOI: 10.1080/014311600210380.

Cao L, Xu JH, Chen YN, Li WH, Yang Y, Hong YL, Li Z, 2012. Understanding the dynamic coupling between vegetation cover and climatic factors in a semiarid region—a case study of Inner Mongolia, China. Ecohydrology. DOI: 10.1002/eco.1245.

Cao XM, Chen X, Bao AM, Wang Q, 2011. Response of vegetation to temperature and precipitation in Xinjiang during the period of 1998–2009. Journal of Arid Land, 3(2): 94–103.

Diodato N, Bellocchi G, 2008. Modelling vegetation greenness responses to climate variability in a Mediterranean terrestrial ecosystem. Environ. Monit. Assess, 143(1–3): 147–159.

Garty J, Tamir O, Hassid I, Eshel A, Cohen Y, Karnieli A, Orlovsky L, 2001. Photosynthesis, chlorophyll integrity and spectral reflectance in lichens exposed to air pollution. Journal of Environmental Quality, 30(3): 884–893.

Giannico C, 2007. Remote sensing of vegetation in the Calabrian region. Acta Astronautica, 60: 119–131.

Hall-Beyer M, 2003. Comparison of single-year and multiyear NDVI time series principal components in cold temperate biomes. IEEE Transac-

tions on Geoscience and Remote Sensing, 41(11): 2568–2574. DOI: 10.1109/TGRS.2003.817274.

Hirosawa Y, Marsh SE, Kliman DH, 1996. Application of standardized principle component analysis to land-cover characterization using multitemporal AVHRR data. Remote Sensing of Environment, 58(3): 267–281. DOI: 10.1016/S0034-4257(96)00068-5.

IGBP, 1997. The terrestrial biosphere and global change: Implications for natural and managed ecosystems. A synthesis of GCTE and related research. IGBP Science, 1: 32. IGBP Secretariat, the Royal Swedish Academy of Sciences, Stockholm, Sweden.

Jakubauskas ME, Legates DR, Kastens JH, 2001. Harmonic analysis of time-series AVHRR NDVI data. Photogrammetric Engineering and Remote Sensing, 67(4): 461–470.

Jarlan L, Mangiarotti S, Mougin E, 2008. Assimilation of SPOT/VEGETATION NDVI data into a Sahelian vegetation dynamics model. Remote Sensing of Environment, 112(4): 1381–1394.

Jonsson P, Eklundh L, 2004. TIMESAT — a program for analyzing time-series of satellite sensor data. Computers & Geosciences, 30(8): 833–845. DOI: 10.1016/j.cageo.2004.05.006.

Li YC, Chen J, Gong P, 2005. Study on land cover change detection method based on NDVI time series datasets: change detection indexes design. Journal of Basic Science and Engineering, 13(3): 261–275.

Lindsay RW, Percival DB, Rothrock DA, 1996. The discrete wavelet transform and the scale analysis of the surface properties of sea ice. IEEE Transactions on Geoscience and Reomote Sensing, 34: 771–787.

Maisongrande P, Duchemin B, Dedieu G, 2004. VEGETATION/SPOT: an operational mission for the Earth monitoring; presentation of new standard products. Int. J. Remote Sens., 25(1): 9–14. DOI: 10.1080/0143116031000115265.

Mallat SG, 1989. A theory for multiresolution signal decomposition: the wavelet representation. IEEE Transactions Pattern Analysis and Machine Intelligence, 11(7): 674–693.

Martínez B, Gilabert MA, 2009. Vegetation dynamics from NDVI time series analysis using the wavelet transform. Remote Sensing of Environment, 113(9): 1823–1842. DOI: 10.1016/j.rse.2009.04.016.

Meyers SD, Kelly BG, O'Brien JJ, 1993. An introduction to wavelet analysis in oceanography and meteorology: with application to the dispersion of Yanai waves. Monthly Weather Review, 121(10): 2858–2866.

Morawitz D, 2006. Using NDVI to assess vegetative land cover change in central Puget Sound. Environmental Monitoring and Assessment, 114(1): 85–106.

Pettorelli N, Vik JO, Mysterud A, Gaillard JM, Tucker CJ, Stenseth NC, 2005. Using the satellite-derived NDVI to assess ecological responses to environmental change. Trends in Ecology & Evolution, 20(9): 503–510. DOI: 10.1016/j.tree.2005.05.011

Sen PK, 1968. Estimates of the regression coefficient based on Kendall's tau. Journal of the American Statistical Association, 63(324): 1379–1389.

Srur AM, Villalba R, Baldi G, 2012. Variations in *Anarthrophyllum rigidum* radial growth, NDVI and ecosystem productivity in the Patagonian shrubby steppes. Plant Ecology, 212: 1841–1854. DOI: 10.1007/s11258-011-9955-6.

Stockli R, Vidale PL, 2004. European plant phenology and climate as seen in a 20-year AVHRR land-surface parameter dataset. International Journal of Remote Sensing, 25(17): 3303–3330. DOI: 10.1080/0143116031000161814 9.

Sun HY, Wang CY, Niu Z, 1998. Analysis of the vegetation cover change and the relationship between NDVI and environmental factors by using NOAA time series data. Journal of Remote Sensing, 2(3): 204–210.

Tucker CJ, Sellers PJ, 1986. Satellite remote sensing of primary production. International Journal of Remote Sensing, 7: 1395–1416.

Turner BL, Lambin EF, Reenberg A, 2007. The emergence of land change science for global environmental change and sustainability. Proceedings of the National Academy of Sciences of the United States of America, 104(52): 20666–20671. DOI: 10.1073/pnas.0704119104.

Xiao J, Moody A, 2005. A comparison of methods for estimating fractional green vegetation cover within a desert-to-upland transition zone in central New Mexico, USA. Remote Sensing of Environment, 98(2–3): 237–250. DOI: 10.1016/j.rse.2005.07.011.

Xu JH, Chen YN, Li WH, Ji MH, Dong S, Hong YL, 2009. Wavelet analysis and nonparametric test for climate change in Tarim River Basin of Xinjiang during 1959–2006. Chinese Geographical Science, 19(4): 306–313. DOI: 10.1007/s11769-009-0306-7.

Xu JH, Chen YN, Li WH, Yang Y, Hong YL, 2011a. An integrated statistical approach to identify the nonlinear trend of runoff in the Hotan River and its relation with climatic factors. Stochastic Environmental Research and Risk Assessment, 25(2): 223–233. DOI: 10.1007/s00477-010-0433-9.

Xu JH, Chen YN, Lu F, Li WH, Zhang LJ, Hong YL, 2011b. The nonlinear trend of runoff and its response to climate change in the Aksu River, western China. International Journal of Climatology, 31(5): 687–695. DOI: 10.1002/joc.2110.

Xu JH, Li WH, Ji MH, Lu F, Dong S, 2010. A comprehensive approach to characterization of the nonlinearity of runoff in the headwaters of the Tarim River, western China. Hydrological Processes, 24(2): 136–146. DOI: 10.1002/hyp.7484.

Xu JH, Lu Y, Su FL, Ai NS, 2004. R/S and wavelet analysis on the evolutionary process of regional economic disparity in China during the past 50 years. Chinese Geographical Science, 14(3): 193–201. DOI: 10.1007/s11769-003-0047-y.

Xu Z, Zhang N, 2006. Long-term trend of precipitation in the Yellow River Basin during the past 50 years. Geographical Research, 25(1): 27–34. DOI: cnki: ISSN: 1000-0585.0.2006-01-003.

Yang ST, Liu CM, Sun R, 2002. The vegetation cover over last 20 years in Yellow River Basin. Acta Geographica Sinica, 57(6): 679–684.

Yang Y, Xu JH, Hong YL, Lv GH, 2012. The dynamic of vegetation coverage and its response to climate factors in Inner Mongolia, China. Stochastic Environmental Research and Risk Assessment, 26(3): 357–373. DOI: 10.1007/s00477-011-0481-9.

Zhang J, Pan XL, Gao ZQ, 2006. Estimation of net primary productivity of the oasis-desert ecosystems in arid west China based on RS-based ecological process. Arid Land Geography, 29(2): 255–261.